Supporting Information

Indole-based A-DA′D-A type acceptor based organic solar cells achieve efficiency over 15% with low energy loss

Yu Chen[a], Rui Cao[a], Hui Liu[a]*, M. L. Keshtov[b], Emmanuel N. Koukaras[c], Hemraj Dahiya[d], Yingping Zou[a], Ganesh D. Sharma[d*]

[a]College of Chemistry and Chemical Engineering, Central South University, Changsha, 410083, P. R. China
[b]Institute of Organoelement Compounds of the Russian Academy of Sciences, Moscow 119991, Russian Federation
[c]Laboratory of Quantum and Computational Chemistry, Department of Chemistry, Aristotle University of Thessaloniki, GR-54124 Thessaloniki, Greece
[d]Department of Physics, The LNM Institute for Information Technology, Jamdoli, Jaipur 302031, India

General Information

^{1}H Nuclear Magnetic Resonance (^{1}H NMR) were recorded by Bruker DMX-400 spectrometer with deuterated chloroform as solvent at 293 K. Chemical shifts were reported as δ values (ppm) with tetramethylsilane (TMS) and $CHCl_3$ (Chemical shift δ = 7.24 ppm for ^{1}H NMR) as the internal references. UV-Vis absorption spectra were recorded on the Shimadzu UV-2600 spectrophotometer. Cyclic voltammetry (CV) was recorded by a computer controlled CHI 660E electrochemical workstation at a scan rate of 20 mV s^{-1} with ID-4F film on platinum electrode (1.0 cm^2) as the working electrode and a platinum wire as the counter electrode as well as Ag/AgCl (0.1 M) as reference electrode in an argon-saturated solution of tetrabutylammonium hexafluorophosphate (0.1 M Bu_4NPF_6 in anhydrous acetonitrile).

Materials

Compounds **1**, **2**, **3**, **4**, and **5** were synthesized according to the previous reported methods[1]. Bis(triphenylphosphine)palladium(II)dichloride ($Pd(PPh_3)_2Cl_2$), tetrahydrofuran (THF), N,N-dimethylformamide (DMF), chloroform ($CDCl_3$) and other reagents were purchased from J&K and Alfa Asia Chemical Co.

Synthesis

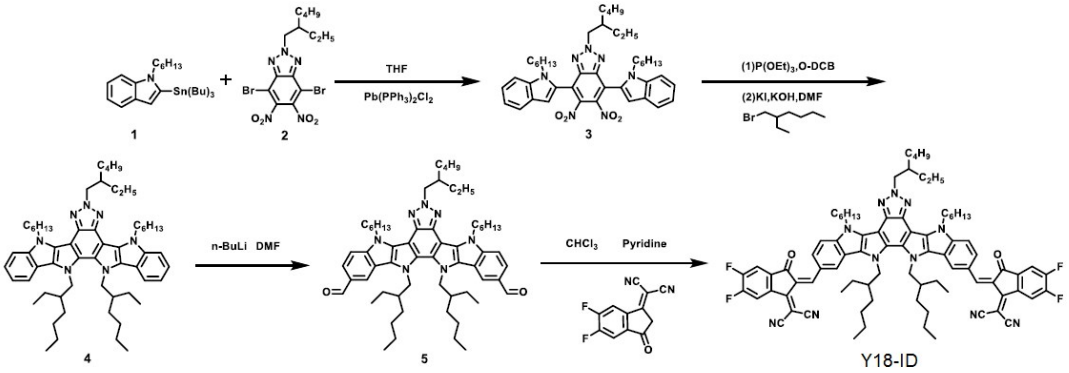

Scheme S1. Synthetic route of **Y18-ID**

Synthesis of 2-(2-ethylhexyl)-4,7-bis(1-hexyl-1H-indol-2-yl)-5,6-dinitro-2H-benzo[d][1,2,3]triazole (3)

1-hexyl-2-(tributylstannyl)-1H-indole(9.74g,19.87mmol), 4,7-dibromo-2-(2-ethylhexyl)-5,6-dinitro-2H-benzo[d][1,2,3]triazole (3.97g, 8.28mmol) and $Pd(PPh_3)_2Cl_2$ (0.30g, 0.41mmol) were dissolved in dry tetrahydrofuran (110 mL) and stirred at 70 °C overnight. The reaction mixture was quenched with water and then cooled to room temperature. After extraction with dichloromethane, the organic phase was concentrated under reduced pressure. The obtained crude product was purified on silica gel chromatography using petroleum ether/CH_2Cl_2 (3:1, v/v) to give compound **3** (6.58g) as a red oil in a yield of 92%.

^{1}H NMR (400 MHz, Chloroform-*d*) δ = 7.66 (d, *J*=7.8, 2H), 7.48 (d, *J*=8.3, 2H), 7.33 (t, *J*=7.6, 2H), 7.18 (t, *J*=7.4, 2H), 6.79 (d, *J*=49.1, 2H), 4.62 (d, *J*=7.1, 2H), 4.14 (ddd, *J*=50.9, 14.7, 7.3, 4H), 2.26 – 2.08 (m, 1H), 1.70 (dt, *J*=37.2, 5.4, 4H), 1.32 – 1.09 (m, 22H), 0.82 (dt, *J*=19.9, 6.2, 10H).

Synthesis of compound 4

Compound **3** (3 g, 4.17 mmol) and triethyl phosphate (50 mL) were dissolved in dichlorobenzene (o-DCB, 20 mL) under nitrogen and then heated at 180 °C for 10 hours. In order to avoid the impact of solvent on the next N-alkylation, o-DCB was removed by vacuum distillation at 90 °C. Subsequently, 3-(bromomethyl)heptane (6.45 g, 33.37 mmol), potassium hydroxide (2.80 g, 50.04 mmol), potassium iodide (1.38g, 8.34mmol) and DMF (80 mL) were added to the mixture and stirred at 90 °C overnight. After cooling to room temperature, the reaction mixture was poured into water. The crude product was extracted by dichloromethane. Further purification was carried out by column chromatography using dichloromethane/petroleum ether (1/10, v / v) as eluent to afford a brown oil **4** (1.65g, 45% yield).

^{1}H NMR (400 MHz, DMSO-*d6*) δ = 7.87 (d, *J*=7.4, 2H), 7.63 (d, *J*=8.1, 2H), 7.23 (t, *J*=7.6, 2H), 7.17 (t, *J*=7.4, 2H), 5.05 – 4.88 (m, 4H), 4.68 (d, *J*=35.7, 6H), 1.93 – 1.81 (m, 6H), 1.61 (s, 4H), 1.26 – 1.21 (m, 18H), 0.95 (q, *J*=7.2, 6H), 0.88 – 0.80 (m, 27H), 0.70 (td, *J*=7.3, 3.7, 6H).

Synthesis of compound 5

Compound **4** (1.65 g, 1.88 mmol) was dissolved in 25 ml of ultra-dry tetrahydrofuran and cooled to -78 °C under argon atmosphere. After stirring at -78 °C for half an hour, n-BuLi (2.59 mL, 1.6 M in hexane) was dropped into the mixture. After stirring for 2 h, ultra-dry DMF (0.35 mL, 4.51 mmol) was quickly added. Subsequently, the reaction mixture was transferred to room temperature and stirred overnight. The reaction was quenched with ice water (300 mL) and extracted with dichloromethane and brine. The obtained crude product was purified on silica gel chromatography using petroleum ether/CH_2Cl_2 (1:1, v/v) to give compound **5** (1.27g) as a red solid in a yield of 72%.

^{1}H NMR (400 MHz, Chloroform-*d*) δ = 10.11 (s, 2H), 8.08 (s, 2H), 7.90 – 7.76 (m, 2H), 7.75 (d, *J*=7.3, 2H), 5.04 (dq, *J*=21.2, 6.8, 4H), 4.69 (t, *J*=7.9, 6H), 2.30 (dt, *J*=25.9, 6.6, 2H), 2.09 – 1.87 (m, 8H), 1.44 (dd, *J*=15.1, 7.8, 11H), 1.32 – 1.21 (m, 26H), 1.00 (t, *J*=7.4, 4H), 0.90 – 0.84 (m, 8H), 0.80 (t, *J*=7.1, 8H).

Synthesis of Y18-ID

Compound **5** (0.20g, 0.21mmol) and 1,1-dicyanomethylene-3-indanone (0.20g, 0.85mmol) and chloroform (30 ml) were placed in a round bottom flask under nitrogen. After stirring for 30 minutes, pyridine (1 mL) was added and stirred at 60 °C overnight. Subsequently, the reaction mixture slowly cooled to room temperature. Chloroform was removed by vacuum distillation. The obtained crude product was purified on silica gel chromatography using petroleum ether/ $CHCl_3$ (1:1.5, v/v) to give compound **Y18-ID** (0.23g) as a dark red solid in a yield of 82%.

^{1}H NMR (400 MHz, Chloroform-*d*) δ = 11.26 (s, 2H), 10.91 (s, 2H), 10.65 – 10.57 (m, 2H), 10.00 (d, *J*=8.4, 2H), 9.90 (d, *J*=8.3, 2H), 9.82 (t, *J*=7.6, 2H), 7.19 (ddd, *J*=29.4, 14.1, 7.1, 4H), 6.85 – 6.72 (m, 6H), 4.42 – 4.33 (m, 1H), 4.25 – 4.17 (m, 4H), 4.08 – 3.99 (m, 2H), 3.70 (s, 6H), 3.63 – 3.51 (m, 12H), 3.43 (d, *J*=7.3, 6H), 3.38 – 3.32 (m, 8H), 3.13 (t, *J*=7.3, 4H), 2.99 (d, *J*=7.1, 6H), 2.92 (d, *J*=7.2, 8H), 2.75 – 2.57 (m, 10H).

The Figures of ^{1}H NMR and mass spectrum

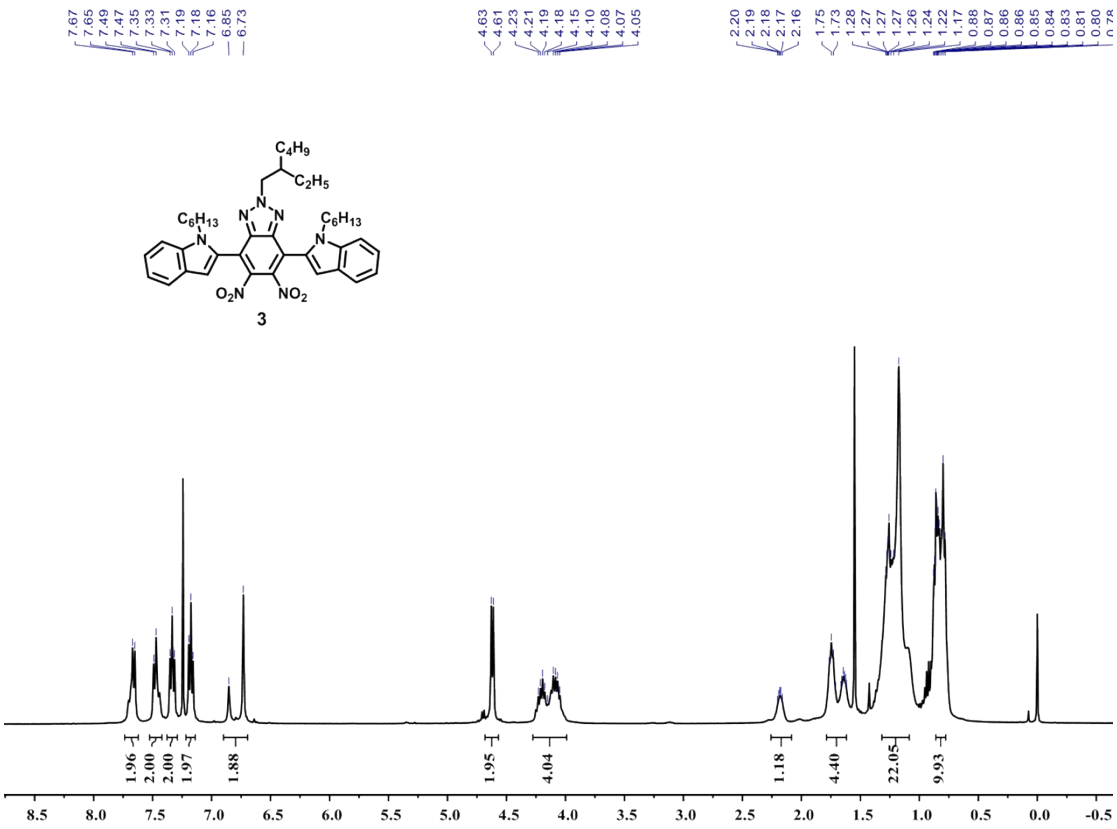

Figure S1. ^{1}H NMR spectrum of compound **3** in $CDCl_3$

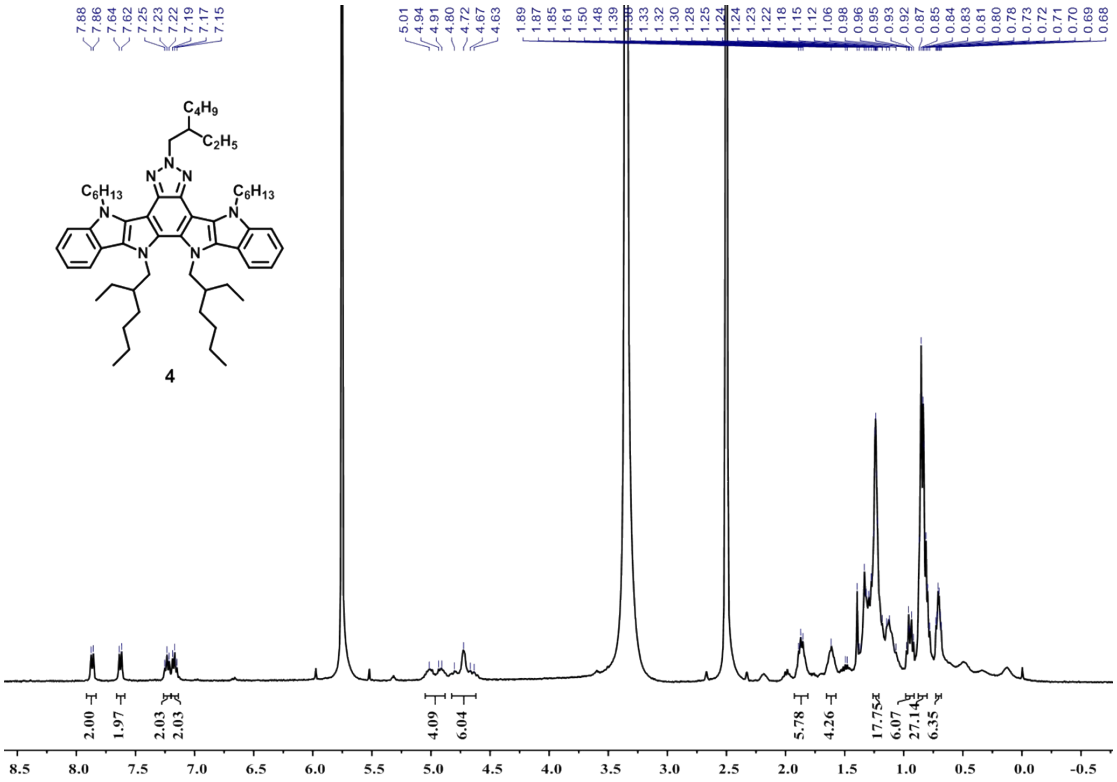

Figure S2. ^{1}H NMR spectrum of compound **4** in DMSO

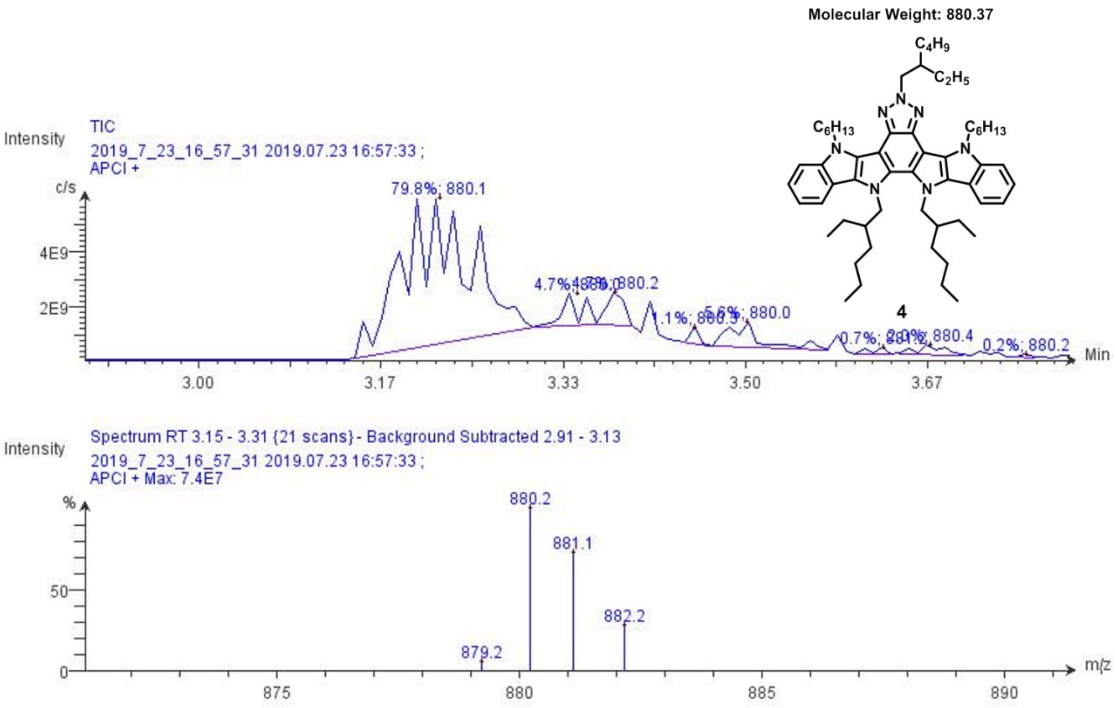

Figure S3. Mass spectrum of compound **4**

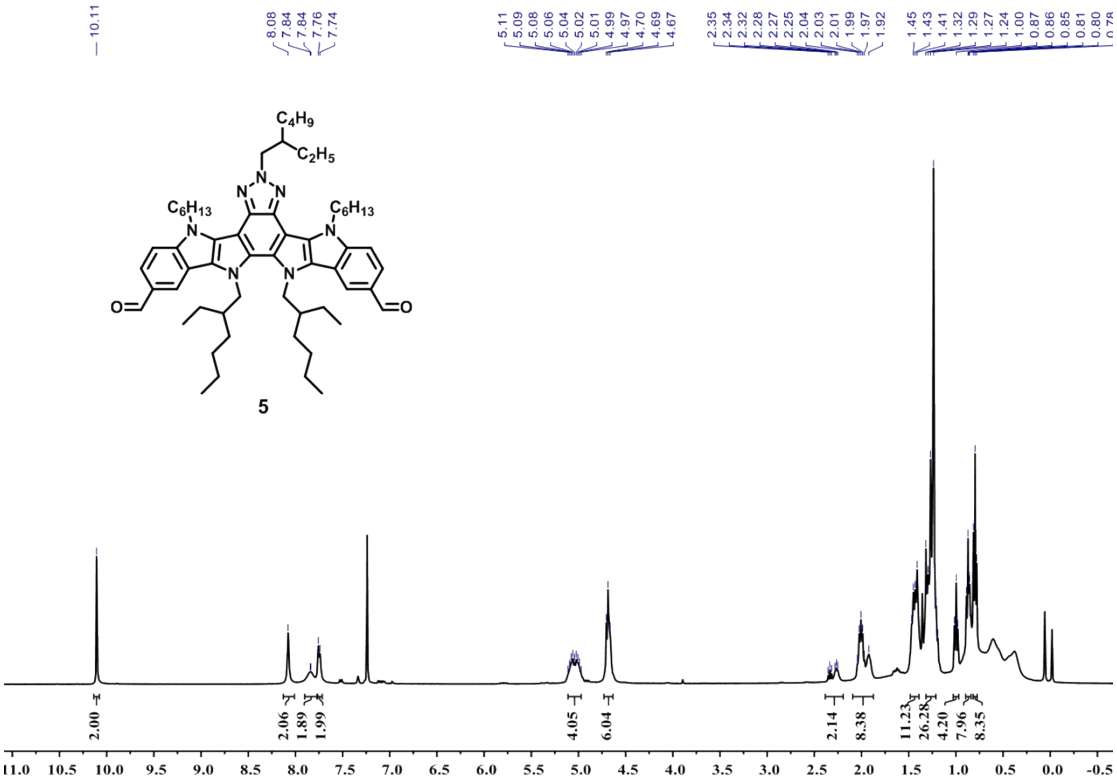

Figure S4. ^{1}H NMR spectrum of compound **5** in $CDCl_3$

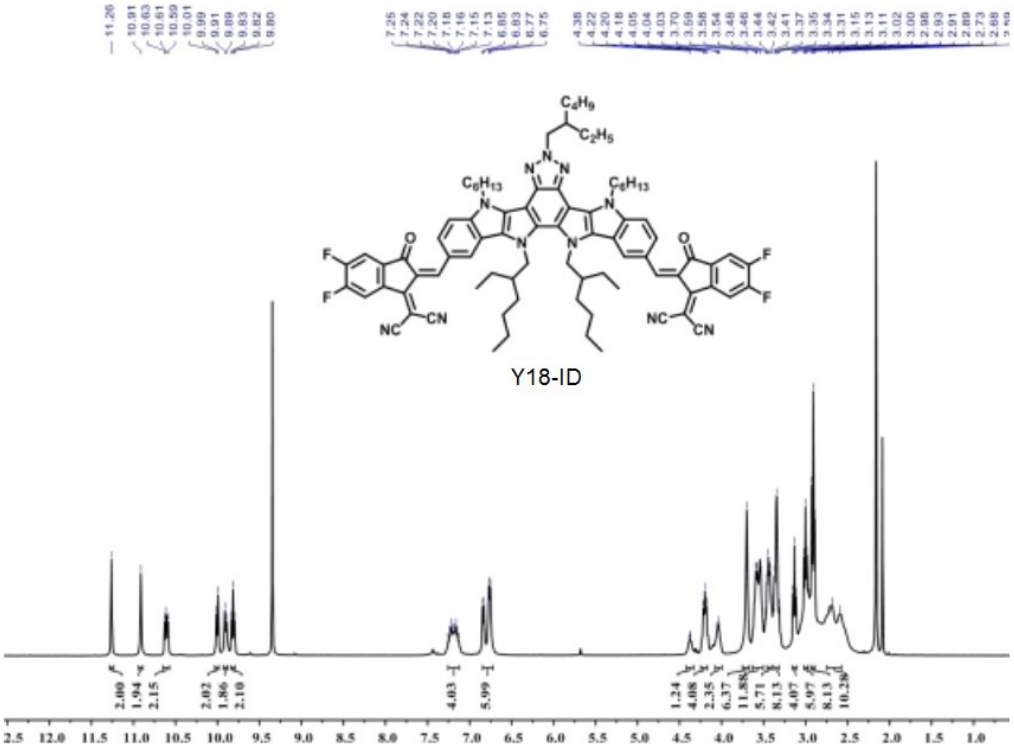

Figure S5. ^{1}H NMR spectrum of **Y18-ID** in $CDCl_3$

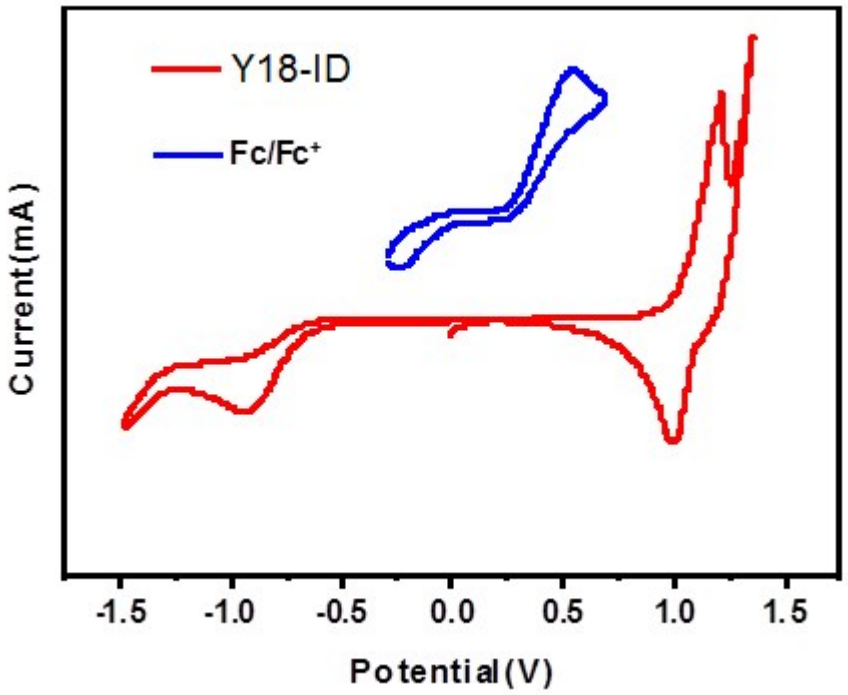

Figure S6 Cyclic voltammetry curve of **Y18-ID**

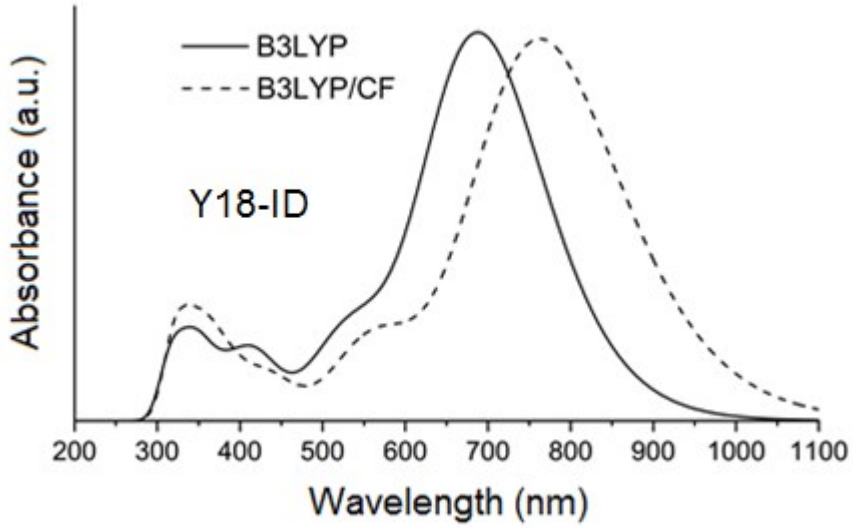

Figure S7 The calculated theoretical UV/Vis absorption spectrum of **Y18-ID** using the B3LYP functional.

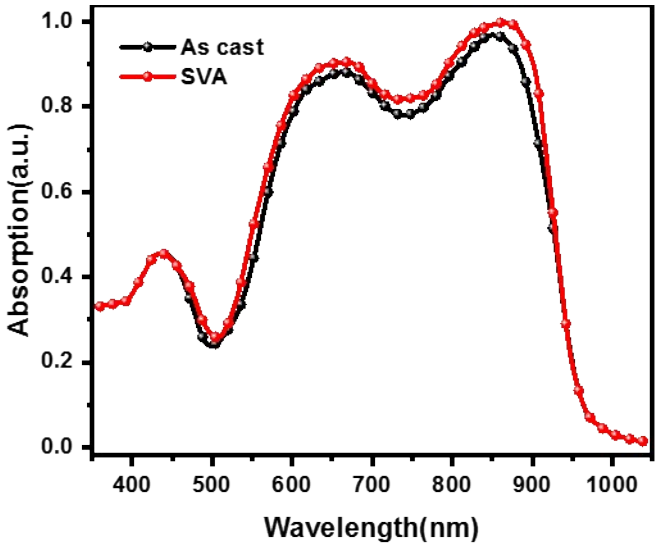

Figure S8 Absorption spectra of the as cast and SVA treated **P:Y18-ID** blend film

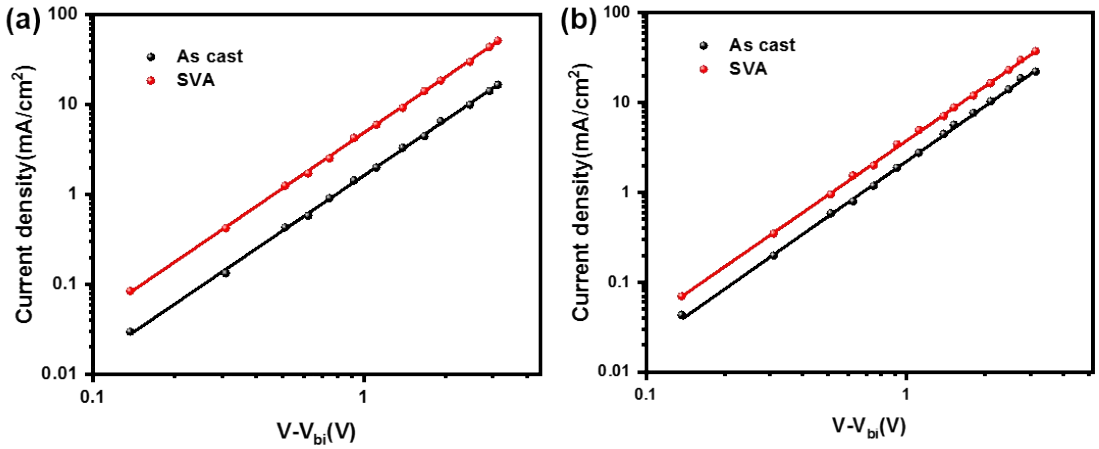

Figure S9 Dark J-V characteristics of the (a) hole only and (b) electron only device. Solid lines denote fitting with space charge limited current model

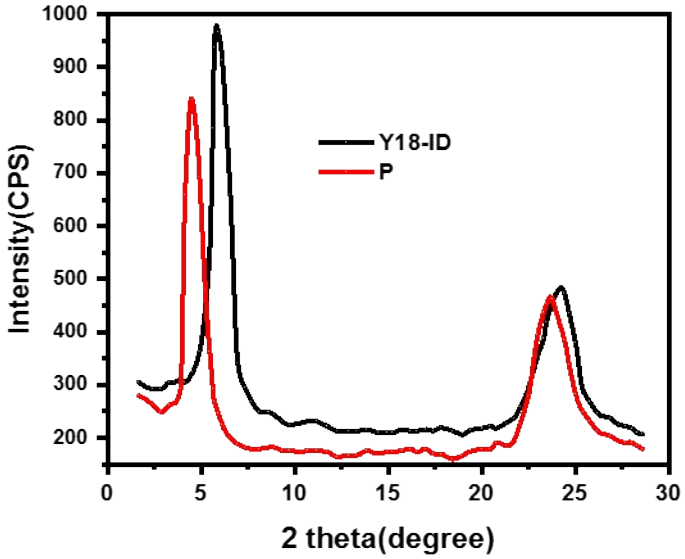

Figure S10 XRD patterns of as cast P and **Y18-ID** films

Details of the Calculations

The initial geometry optimization calculations were performed employing the gradient corrected functional PBE [2] of Perdew, Burke and Ernzerhof. The def-SVP basis set [3] was used for all of the calculations. At this stage of the calculations, to increase the computational efficiency (without loss in accuracy), the resolution of the identity method [4] was used for the treatment of the two-electron integrals. Subsequent geometry optimizations were further performed using the hybrid exchange–correlation functional B3LYP [5] and Truhlar's meta-hybrid exchange–correlation functional M06 [6] with the same basis set. Solvent effects were simulated with chloroform (CF) using the integral equation formalism variant of the Polarizable Continuum Model (IEFPCM), as implemented in the Gaussian package. [7] Tight convergence criteria were placed for the SCF energy (up to 10–7 Eh) and the one-electron density (rms of the density matrix up to 10^{-8}) as well as the norm of the Cartesian gradient (residual forces both average and maximum smaller than 1.5×10^{-5}

a.u.) and residual displacements (both average and maximum smaller than 6×10^{-5} a.u.).

Vibrational analysis on all of the optimized structures did not reveal any vibrational modes with imaginary eigen frequencies, i.e. The final optimized structures are true local (if not global) minima. In addition to the B3LYP functional, we have also performed our calculations employing the M06 functional. The M06 meta-hybrid functional was chosen since it provides leveled performance over transition types. [8],[9] We provide results using all three functionals, which can additionally be used for comparison with the literature. The UV/Visual spectra have been obtained by convoluting Gaussian functions with HWHM = 0.22 eV centered at the excitation wavenumbers.

Device fabrication and characterization

We have fabricated the OSCs using a conventional structure of ITO/PEDOT:PSS/active layer/PFN/Al. The ITO glass was cleaned by ultra-sonication using detergent, deionized water and iso-propyl alcohol, sequentially and then dried in vacuum oven for overnight. After cleaning and drying, a thin film of PEDOT:PSS (40 nm) was spin coated (3000 rpm for 20 s) in ambient condition and annealed at 120 °C to form the HTL of 40 nm. The prepared active solution of different donor to acceptor weight ratio of polymer P and **Y18-ID** were prepared with total concentration of 16 mg/mL and then spin coated (2500 rpm for 30 s) onto the top of PEDOT:PSS layer and dried at room temperature for 30 min. For the solvent vapour annealing (SVA) treatment, the optimized active layer was placed in THF environment for different times. The thickness of the active layers are 90 ± 5 nm. The thin film of PFN (10 nm) was spin coated (3500 rpm) for 10 s on the top of active layer from methanol solution to form the ET. Finally, aluminum (Al) electrode was deposited on the top of PFN film through thermal evaporation with high vacuum

chamber (under 1×10^{-5} torr). The active area of the devices is 16 mm^2. The current - voltage (J-V) characteristics of the fabricated OSCs were measured by Keithely 2400 source meter and solar simulator (AM1.5G, 100 mW/cm^2). Incident photon to current conversion efficiency (IPCE) was recorded using Bentham IPCE system. The hole and electron mobilities were estimated using the space charge limited current (SCLC) model with fabricating the hole (ITO/PEDOT:PSS/active layer/Au) and electron (ITO/Al/active layer/Al) only devices, respectively.

Table S1**.** Electronic excitations of **Y18-ID** (with non-negligible oscillator strengths, *f*), and the corresponding major contributions. Calculated using the M06 functional (and CF for solvent).

No.	Wavelength (nm)	f	Main Contributions
1	705	2.709	H□L (96%)
2	601	0.027	H□L+1 (87%), H–1□L (11%)
3	571	0.020	H–1□L (83%), H□L+1 (11%)
4	528	0.036	H–1□L+1 (72%), H–2□L (22%)
5	519	0.318	H□L+2 (93%)
7	470	0.117	H–2□L (72%), H–1□L+1 (24%)
10	431	0.011	H–1□L+2 (73%)
11	422	0.011	H–1□L+3 (83%)
12	408	0.232	H–3□L+1 (82%)
13	374	0.047	H–2□L+2 (79%)
16	366	0.082	H□L+4 (58%), H–5□L (15%)
17	361	0.010	H–2□L+3 (40%), H–4□L (24%), H–3□L+2 (10%),
22	346	0.073	H–9□L (37%), H–10□L+1 (26%), H–6□L (12%)
24	344	0.308	H–6□L (42%), H–9□L (10%), H–3□L+2 (13%), H–5□L+1 (10%),

26	336	0.182	H–7□L (47%), H–3□L+3 (23%)
28	327	0.167	H–1□L+4 (88%)
29	317	0.011	H–6□L+1 (17%), H–6□L+3 (14%), H–5□L+2 (13%), H–7□L+2 (12%), H–8□L (11%)
30	316	0.271	H–6□L+2 (26%), H□L+5 (16%), H–7□L+3 (13%)
33	309	0.017	H□L+6 (71%)
34	309	0.229	H□L+5 (68%)
35	304	0.022	H–6□L+1 (41%), H–7□L (26%), H–5□L+2 (10%)
36	303	0.046	H–4□L+2 (77%)
39	298	0.023	H–2□L+4 (57%), H–5□L+2 (15%)
40	295	0.183	H–5□L+3 (18%), H–13□L (14%)

Table S2 Photovoltaic parameters of the OSCs based on P:**Y18-ID** with different weight ratios

Weight ratio	J_{sc} (mA/cm^2)	V_{oc} (V)	FF	PCE (%)
1:0.4	19.15	0.89	0.56	9.54
1:0.8	20.47	0.88	0.58	10.45
1:1.2	21.09	0.87	0.61	11.19
1:1.5	**21.78**	**0.88**	**0.64**	**12.27**
1.1:1.6	21.34	0.87	0.61	11.32

Table S3 Photovoltaic parameters of the OSCs based on SVA treated P:**Y18-ID** with different exposure time

SVA time	J_{sc} (mA/cm^2)	V_{oc} (V)	FF	PCE (%)
20 s	23.15	0.86	0.69	12.55
30 s	24.08	0.84	0.72	14.56
40 s	**24.53**	**0.84**	**0.74**	**15.25**
50 s	24.11	0.82	0.72	14.23

Table S4 Summary of the photovoltaic performance of non-fullerene acceptors based binary OPVs with efficiencies over 13% and E_{loss} below 0.6 eV.

Active layer	V_{oc}	J_{sc}	FF	PCE	E_{loss}[a]	Ref
PBDB-T:INPIC-4F	0.85	21.61	71.50	13.13	0.54	10
FTAZ:IDCIC	0.87	21.98	71.03	13.58	0.56	11
PBDB-T:SN6IC-4F	0.78	23.20	73.00	13.20	0.55	12
PBDB-T-SF:NCBDT-4C	0.85	22.35	74.30	14.10	0.57	13
PM6:Y6	0.83	25.30	74.80	15.70	0.57	14
PM7:IDT6CN-M	1.05	16.40	77.50	13.30	0.58	15
J101:ZITI	0.94	21.25	72.48	14.43	0.57	16
PBDB-TF:AQx-1	0.89	22.18	67.14	13.31	0.45	17
PM6:Y18	0.84	25.71	76.50	16.52	0.53	18
PTQ10:Y6	0.83	26.65	75.10	16.53	0.54	19
PM6:BTP-4Cl	0.87	25.40	75.00	16.50	0.53	20
PBDB-T:Y1	0.87	22.44	69.10	13.42	0.57	21
PBDB-T:Y2	0.82	23.56	69.40	13.40	0.57	22
PBDB-T:Y5	0.87	22.60	71.40	14.00	0.51	23
PBDB-T:Y9	0.90	23.38	63.00	13.26	0.46	24
PM6:Y11	0.83	26.74	74.33	16.54	0.56	25
PM6:Y15	0.87	23.79	68.49	14.13	0.55	26
PM6:Y21	0.83	24.90	74.40	15.40	0.52	27
PTQ11:TPT10	0.88	24.79	74.80	16.32	0.48	28

P:Y18-ID	0.84	24.53	74.00	15.25	0.51	This work

[a] $E_{loss} = E_g/q - V_{oc}$, wherein $E_g = 1240/\lambda_{onset}$, q is the elementary charge.

Reference

1. J. Yuan, Y. Zhang, L. Zhou, G. Zhang, H. L. Yip, T. K. Lau, X. Lu, C. Zhu, H. Peng, P. A. Johnson, M. Leclerc, Y. Cao, J. Ulanski, Y. Li and Y. Zou, *Joule*, 2019, **3**, 1140-1151

2. J. P. Perdew, K. Burke and Ernzerhof, M. *Phys. Rev. Lett.* 1996, **77**, 3865–3868.

3 A. Schafer, H. Horn and R. Ahlrichs, *J. Chem. Phys.* 1992, **97**, 2571.

4. K. Eichkorn, O. Treutler, H. Öhm, M. Häser and R. Ahlrichs, *Chem. Phys. Lett.* 1995, **240**, 283.

5. (a) A. D. Becke, *J. Chem. Phys.* 1993, 98, 5648–5652. (b) C. Lee, W. Yang and R. G. Parr, *Phys. Rev. B* 1988, **37**, 785–89.

6. Y. Zhao and D. G. Truhlar, *Theor. Chem. Acc.* 2008, **120**, 215–241.

7. Frisch, M. J.; Trucks, G. W.; Schlegel, H. B.; Scuseria, G. E.; Robb, M. A.; Cheeseman, J. R.; Scalmani, G.; Barone, V.; Mennucci, B.; Petersson, G. A.; Nakatsuji, H.; Caricato, M.; Li, X.; Hratchian, H. P.; Izmaylov, A. F.; Bloino, J.; Zheng, G.; Sonnenberg, J. L.; Hada, M.; Ehara, M.; Toyota, K.; Fukuda, R.; Hasegawa, J.; Ishida, M.; Nakajima, T.; Honda, Y.; Kitao, O.; Nakai, H.; Vreven, T.; Montgomery, Jr., J. A.; Peralta, J. E.; Ogliaro, F.; Bearpark, M.; Heyd, J. J.; Brothers, E.; Kudin, K. N.; Staroverov, V. N.; Kobayashi, R.; Normand, J.; Raghavachari, K.; Rendell, A.; Burant, J. C.; Iyengar, S. S.; Tomasi, J.; Cossi, M.; Rega, N.; Millam, J. M.; Klene, M.; Knox, J. E.; Cross, J. B.; Bakken, V.; Adamo, C.; Jaramillo, J.; Gomperts, R.; Stratmann, R. E.; Yazyev, O.; Austin, A. J.; Cammi, R.; Pomelli, C.; Ochterski, J. W.; Martin, R. L.; Morokuma, K.; Zakrzewski, V. G.; Voth, G. A.; Salvador, P.; Dannenberg, J. J.; Dapprich, S.; Daniels, A. D.; Farkas, Ö.; Foresman, J. B.; Ortiz, J. V.; Cioslowski, J.; Fox, D. J. Gaussian 03, revision C.01; Gaussian, Inc.: Wallingford CT, 2004.

8. D. Jacquemin, E. A. Perpète, I. Ciofini, Adamo; R. Valero, Y. Zhao and D. G. Truhlar, *J. Chem. Theory Comput.* 2010, **6**, 2071–2085.

9. S. Mathew, A. Yella, P. Gao, R. Humphry–Baker, F. E. Curchod, N. Ashari–Astani, I. Tavernelli, U. Rothlisberger, M. K. Nazeeruddin, M. Grätzel, *Nature Chem.* 2014, **6**, 242–247.

10 D. He, F. Zhao, J. Xin, J. J. Rech, Z. Wei, W. Ma, W. You, B. Li, L. Jiang and Y. Li, Adv. Energy Mater., 2018, **8**, 1802050.
11 C. Huang, X. Liao, K. Gao, L. Zuo, F. Lin, X. Shi, C.-Z. Li, H. Liu, X. Li and F. Liu, Chem. Mat., 2018, **30**, 5429-5434.
12 B. Kan, H. Feng, H. Yao, M. Chang, X. Wan, C. Li, J. Hou and Y. Chen, Sci. China-Chem., 2018, **61**, 1307-1313.
13 J. Yuan, Y. Zhang, L. Zhou, G. Zhang, H.-L. Yip, T. K. Lau, X. Lu, C. Zhu, H. Peng, P. A. Johnson, M. Leclerc, 14 Y. Cao, J. Ulanski, Y. Li and Y. Zou, Joule, 2019, **3**, 1140-1151.
15 Q. Fan, T. Liu, W. Gao, Y. Xiao and Y. Li, J. Mater. Chem. A, 2019, **7**, 15404-15410.
16 T. Wang, R. Sun, S. Xu, J. Guo, W. Wang, J. Guo, X. Jiao, J. Wang, S. Jia and X. Zhu, J. Mater. Chem. A, 2019, **7**, 14070-14078.
17 W. Liu, J. Zhang, S. Xu and X. Zhu, Sci. Bull., 2019, **64**, 1144-1147.
18 C. Zhu, J. Yuan, F. Cai, L. Meng, H. Zhang, H. Chen, J. Li, B. Qiu, H. Peng, S. Chen, Y. Hu, C. Yang, F. Gao, Y. Zou and Y. Li, Energy Environ. Sci., 2020, **13**, 2459-2466.
19 Y. Wu, Y. Zheng, H. Yang, C. Sun, Y. Dong, C. Cui, H. Yan and Y. Li, Sci. China-Chem., 2019, **63**, 265-271.
20 Y. Cui, H. Yao, J. Zhang, T. Zhang, Y. Wang, L. Hong, K. Xian, B. Xu, S. Zhang, J. Peng, Z. Wei, F. Gao and J. Hou, Nat. Commun., 2019, **10**, 2515.
21 J. Yuan, T. Huang, P. Cheng, Y. Zou, H. Zhang, J. L. Yang, S.-Y. Chang, Z. Zhang, W. Huang, R. Wang, D. Meng, F. Gao and Y. Yang, Nat. Commun., 2019, **10**, 570.
22 J. Yuan, Y. Zhang, L. Zhou, C. Zhang, T. K. Lau, G. Zhang, X. Lu, H. L. Yip, S. K. So, S. Beaupré, M. Mainville, P. A. Johnson, M. Leclerc, H. Chen, H. Peng, Y. Li and Y. Zou, Adv. Mater., 2019, **31**, 1807577.
23 M. Luo, L. Zhou, J. Yuan, C. Zhu, F. Cai, J. Hai and Y. Zou, J. Energy Chem., 2020, **42**, 169-173.
24 S. Liu, J. Yuan, W. Deng, M. Luo, Y. Xie, Q. Liang, Y. Zou, Z. He, H. Wu and Y. Cao, Nat. Photonics, 2020, **14**, 300-305.
25 M. Luo, C. Zhu, J. Yuan, L. Zhou, M. L. Keshtov, D. Y. Godovsky and Y. Zou, Chin. Chem. Lett., 2019, **30**, 2343-2346.
27 F. Cai, C. Zhu, J. Yuan, Z. Li, L. Meng, W. Liu, H. Peng, L. Jiang, Y. Li and Y. Zou, Chem. Commun., 2020, **56**, 4340-4343.
28 C. Sun, S. Qin, R. Wang, S. Chen, F. Pan, B. Qiu, Z. Shang, L. Meng, C. Zhang, M. Xiao, C. Yang and Y. Li, J. Am. Chem. Soc., 2020, **142**, 1465-1474.